Implementing PGD technique in solving the problem of identifying Young's modulus of linear elastic isotropic material from full-field measurements by FEMU method

Nguyen Hai Nam*, Phung Van Binh

Faculty of Aerospace Engineering, Le Quy Don Technical University, Hanoi, Vietnam;
*Corresponding author: hai_nam.nguyen@lqdtu.edu.vn
Received 02 Jul. 2023; Revised 21 Aug. 2023; Accepted 30 Aug. 2023; Published 25 Nov. 2023.
DOI: https://doi.org/10.54939/1859-1043.j.mst.91.2023.96-105

ABSTRACT

This paper deals with implementing Proper Generalized Decomposition (PGD) technique in solving the problem of identifying Young's modulus of linear elastic isotropic material from full-field measurements by finite element model updating (FEMU) method. In this type of problem, using PGD technique enables reducing the computation cost as it helps to avoid performing the iterative process of computing the response of the mechanical structure by finite element method (FEM). The nature of PGD technique consists following important points: (i) – Interested parameters are considered as extra variables for the response function; (ii) – Sought multidimensional response function is approximated by the finite sum of modes, each is production of separated-variable functions; (iii) – This approximate solution is computed by the iterative solver using a variational formulation and a greedy algorithm. A numerical example of a tensile test was performed to verify this implementation. The obtained results confirm the correctness of PGD technique. Several comments were made on the use of this technique.

Keywords: Material parameter identification problem; Finite element method updating (FEMU) method; Proper generalized decomposition (PGD) technique.

1. INTRODUCTION

1.1. Parameter identification

In the field of mechanics, to design a structure or to numerically simulate the response of a structure subjected to given loadings, structural parameters such as geometrical parameters, materials parameters, boundary conditions need to be given. Material parameters (for example Young's modulus and Poisson's ratio for linear elastic material) are identified in the earlier phase by solving the so-called material parameter identification problem. This is an inverse problem in solid mechanics where the material parameters are identified based on data obtained in mechanical tests, [1]. Techniques to obtain experimental data can be divided into 2 groups: (i) contact and (ii) non-contact measurement techniques. In contact techniques [2, 3], kinematic field variables such as displacements or strains are usually measured by means of localized sensors (e.g. strain gauges) mounted directly on the structures. On the other hand, non-contact techniques use high-speed CCD cameras to capture the state of the testing sample at different moments. These techniques of measurement are also called full-field measurement techniques as they enable to retrieve full-field experimental data in the form of 2D or 3D images, meaning that pixels are sensors. To obtain kinematic field variables (displacements or strains), the obtained images need to be processed by different techniques such as digital image correlation (DIC) [4], digital volume correlation (DVC) [5], etc. Based on these kinematic fields, material parameters can be identified using several methods such as the finite element model updating method (FEMU), the

constitutive equation gap method (CEGM), the virtual fields method (VFM), the equilibrium gap method (EGM), the reciprocity gap method (RGM) [5], the mCRE method [6], etc. Among those methods, FEMU [5, 7] is the most popular and widely employed in practical applications; it consists in performing iteratively finite element simulations of the test to find material parameters so that the corresponding computed response of the structure matches at best the actual measurements.

An important problem related to numerical simulation is the computational cost. Large-size problems can take an enormous amount of time to solve even using the most advanced computing facilities. In such situation, reduced order modeling (ROM) reduction techniques can be used. There are three ROM techniques: the proper orthogonal decomposition (POD) method [8], the Reduced Basis (RB) method [9]; the PGD method [10].

PGD technique consists of seeking the multidimensional solution in a low-rank modal approximation form, i.e. a finite sum of modes, each is production of separated-variable functions. Additional model parameters (related to material properties, boundary conditions, geometry etc.) can also be inserted as extra-variables of the problem. This approximate solution is computed by the iterative solver using a variational formulation and a greedy algorithm.

During the last decade, PGD technique was extensively used to solve multidimensional problems and perform efficient simulation [11]. In the field of mechanics, PGD technique was applied to study the crack propagation in brittle materials [12], Piezoelectric & Magnetostrictive Materials [13], composite materials [14], woven composite materials [15]. For material parameter identification problem, PGD technique was used in combination with mCRE method in [6, 17]. To our limited knowledge, there is no publication on a combination of PGD technique and FEMU approach to solve the material parameter identification problem based on full-field measurements. Thus, in this work, this problem was addressed, particularly in solving the problem of identifying Young's modulus of linear elastic isotropic material from full-field measurements by FEMU method.

2. METHODOLOGY

2.1. The DIC procedure

The purpose of DIC is to extract the displacement field $\mathbf{u}_{dic}(\mathbf{x})$ that best matches between two images: (i) a reference image $f(\mathbf{x})$; (ii) a deformed image $g(\mathbf{x})$. Each image is a set of pixels ($\mathbf{x}$ denotes the pixel coordinates) with the distribution of light intensity or gray level values. In the ideal case, when the images are acquired without noise, the local gray-level conservation can be $g(\mathbf{x}) = f(\mathbf{x} + \mathbf{u}_{dic}(\mathbf{x}))$. However, in reality, image acquisition is never perfect, and always contains a small amount of noise $\eta(\mathbf{x})$, which is often considered as Gaussian and “white”, or spatially uncorrelated, so that $g(\mathbf{x}) = f(\mathbf{x} + \mathbf{u}_{dic}(\mathbf{x})) + \eta(\mathbf{x})$. In this case, $\mathbf{u}_{dic}(\mathbf{x})$ can be calculated by minimizing the global correlation residual defined as a quadratic difference of reference and deformed images as follows (where ROI stands for "region of interest"):

$$\Phi^2 = \int_{ROI} \left[g(\mathbf{x}) - f(\mathbf{x} + \mathbf{u}_{dic}(\mathbf{x})) \right]^2 d\mathbf{x} \quad (1)$$

The details of solving this minimazation problem can be found in [4]. Due to the noise, the solution $\mathbf{u}_{dic}(\mathbf{x})$ of this problem is not the exact displacement field. Instead, it is the noisy solution which can be expressed as sum of exact solution $\mathbf{u}_{ex}(\mathbf{x})$ and the displacement noise $\boldsymbol{\eta}_{\mathbf{u}}(\mathbf{x})$.

2.2. The DIC-FEMU method

The goal of the DIC-FEMU approach is to identify the vector of constitutive parameters $\mathbf{p}$ that achieves the best match between computed by FEM displacement $\mathbf{u}_{fem}(\mathbf{x},\mathbf{p})$ and measured displacement $\mathbf{u}_{dic}(\mathbf{x})$, defined by DIC technique. It consists in minimizing a chosen cost function. A choice of the cost function can be of the form (2) ([5]) where $\mathbf{U}_{fem}(\mathbf{x},\mathbf{p})$ and $\mathbf{U}_{dic}(\mathbf{x})$ are the vectors of nodal values of $\mathbf{u}_{fem}(\mathbf{x},\mathbf{p})$ and $\mathbf{u}_{dic}(\mathbf{x})$, respectively; $\mathbb{W}$ is weighting matrix (for the sake of simplicity, in this work, $\mathbb{W}$ is chosen equal to an identity matrix).

$$J(\mathbf{p})=\frac{1}{2}\left[\mathbf{U}_{fem}(\mathbf{x},\mathbf{p})-\mathbf{U}_{dic}(\mathbf{x})\right]^{T}\mathbb{W}\left[\mathbf{U}_{fem}(\mathbf{x},\mathbf{p})-\mathbf{U}_{dic}(\mathbf{x})\right] \tag{2}$$

This problem is solved iteratively according to following algorithm:

1. Given tolerance value TOL and assign $k=1$;
2. Initiate $\mathbf{p}^{(k)}$;
3. Compute $\mathbf{U}_{fem}(\mathbf{x},\mathbf{p}^{(k)})$ by FEM;
4. Compute $J(\mathbf{p}^{(k)})$;
5. Check $J(\mathbf{p}^{(k)})<TOL$;
   a. If yes: Go to step 6;
   b. If no: $k=k+1$; Update $\mathbf{p}^{(k)}=\mathbf{p}^{(k-1)}+\boldsymbol{\delta}\mathbf{p}^{(k)}$ and go back to step 3.
6. Choose $\mathbf{p}=\mathbf{p}^{(k)}$ as solution.

2.3. The PGD technique

The standard approach to compute PGD modes is the so-called *progressive Galerkin* approach. This approach was also explained in [6]. In this section, the specific implementation of this technique to solve the linear elasticity problem is detailed.

2.3.1. Reference linear elasticity problem

Consider a generic elastic body whose undeformed configuration occupies the domain Ω subjected to a body force $\mathbf{b}$ on Ω and a surface force $\mathbf{f}$ on a part Γ_N of the boundary $\partial\Omega$ of Ω. On the complement part Γ_D of the boundary $\partial\Omega$ ($\Gamma_D\cup\Gamma_N=\partial\Omega$ and $\Gamma_D\cap\Gamma_N=\varnothing$), a Dirichlet boundary condition is prescribed. The virtual work principle for three sets of governing equations (the equilibrium equations, the kinematic compatibility equations, and the constitutive equation) for this system reads:

$$\int_{\Omega}\boldsymbol{\sigma}\cdot\boldsymbol{\varepsilon}(\boldsymbol{\delta}\mathbf{v})=\int_{\Omega}\mathbf{b}\cdot\boldsymbol{\delta}\mathbf{v}+\int_{\Gamma_N}\mathbf{f}\cdot\boldsymbol{\delta}\mathbf{v} \tag{3}$$

In equation (3), $\boldsymbol{\sigma}=\mathbb{C}\boldsymbol{\varepsilon}(\mathbf{u})$ where $\boldsymbol{\varepsilon}$ and $\boldsymbol{\sigma}$ are the Voigt notations of infinitesimal

strain tensor and the Cauchy stress tensor, $\mathbb{C}$ is Hooke's stiffness matrix; $\mathbf{u}$ is the displacement vector; $\boldsymbol{\delta}\mathbf{v}$ is the arbitrary test function, which satisfies the Dirichlet boundary condition. In the following, for simplicity, the body force is assumed to be absent ($\mathbf{b} = 0$). The equation (3) becomes:

$$\int_{\Omega} \mathbb{C}\boldsymbol{\varepsilon}(\mathbf{u}) \cdot \boldsymbol{\varepsilon}(\boldsymbol{\delta}\mathbf{v}) = \int_{\Gamma_N} \mathbf{f} \cdot \boldsymbol{\delta}\mathbf{v} \tag{4}$$

2.3.2. Direct problem

The direct problem consists of determining the displacement, strain and stress fields given the geometry of the solid, the constitutive parameters, boundary conditions and the loadings from equation (4). Closed-form solutions to direct problem is available only in very particular cases. Hence numerical solution techniques are usually called for; the most commonly used technique is the FEM. The usual Galerkin discretization procedure using FEM shape functions provides the standard set of FEM equations $\mathbb{K}_{fem}\mathbf{U}_{fem} = \mathbf{F}$ where: $\mathbb{K}_{fem}$ is the global FEM stiffness matrix, restricted to the non-prescribed degrees of freedom (DOFs); $\mathbf{F}$ is the generalized load vector, and $\mathbf{U}_{fem}$ is the unknown vector of nodal displacements introduced by the FEM discretization. In each iteration of DIC-FEMU method, at step 3, $\mathbf{U}_{fem}$ is calculated from this equation. It can be seen that, given the constitutive parameters, $\mathbf{U}_{fem}$ only depends on the space coordinates $\mathbf{x}$.

2.3.3. Implementation of PGD technique

When using PGD technique, the displacement field $\mathbf{u}$ is sought in the form of a finite sum of modes, each is production of separated-variable functions. Besides the main variable **x**, any model parameter such as material properties, boundary conditions, geometry, etc. can be used as extra variable. Specifically, the approximate PGD form of $\mathbf{u}$ is:

$$\mathbf{u}^m(\mathbf{x}, p_1, p_2 \ldots p_P) = \sum_{i=1}^{m} \boldsymbol{\rho}_i(\mathbf{x}) \prod_{j=1}^{P} \chi_i^j(p_j) \tag{5}$$

where P is the number of extra variables, p_j $(j = 1 \ldots P)$ are the extra variables.

There are some advantages of PGD form of $\mathbf{u}$: (i) the explicit dependency of $\mathbf{u}^m$ on parameters p_j $(j = 1 \ldots P)$ enables to compute very fast the value of $\mathbf{u}^m$ at any values of p_j; (ii) the decomposition of multidimensional function into a combination of separated-variable functions enables grouping the functions of the same variable; this is helpful for taking integral when solving the problem in the variational formulation.

In this work, only 1 extra parameter ($P = 1$) which is Young's modulus E was considered. Therefore, the PGD form of sought displacement is:

$$\mathbf{u}^m = \sum_{i=1}^{m-1} \boldsymbol{\rho}_i e_i + \boldsymbol{\rho}_m e_m = \mathbf{u}^{m-1} + \boldsymbol{\rho}_m e_m \tag{6}$$

where $\mathbf{u}^i = \mathbf{u}^i(\mathbf{x}, E)$; $\boldsymbol{\rho}_i = \boldsymbol{\rho}_i(\mathbf{x})$ is the space function and $e_i = e_i(E)$ is the Young's modulus dependent function. The test functions $\boldsymbol{\delta}\mathbf{v}$ was chosen in the tangent space:

$$\boldsymbol{\delta}\mathbf{v} = \boldsymbol{\delta}\mathbf{v}^{\boldsymbol{\rho}} + \boldsymbol{\delta}\mathbf{v}^{e} \text{ where } \boldsymbol{\delta}\mathbf{v}^{\boldsymbol{\rho}} = \boldsymbol{\delta}\boldsymbol{\rho}_m e_m; \quad \boldsymbol{\delta}\mathbf{v}^{e} = \boldsymbol{\rho}_m \delta e_m$$

For the elasticity problem, the plane stress Hooke's matrix can be written in the separation form $\mathbb{C} = E\mathbb{C}_\nu$ where $\mathbb{C}_\nu$ is the matrix depending only on Poisson's ratio.

Substitute all of these to equation (4) and taking integral over the considered inteval I_E of Young's modulus value, the following system of 2 equations was obtained, where the first equation is the space problem (obtained by substituting $\boldsymbol{\delta v} = \boldsymbol{\delta v}^{\boldsymbol{\rho}}$) and the second equation is the Young's modulus-related problem (obtained by substituting $\boldsymbol{\delta v} = \boldsymbol{\delta v}^{e}$):

$$\begin{cases} \sum_{i=1}^{m-1} \int_{I_E} \int_{\Omega} E\mathbb{C}_\nu \boldsymbol{\varepsilon}(\boldsymbol{\rho}_i e_i) \cdot \boldsymbol{\varepsilon}(\boldsymbol{\delta\rho}_m e_m) + \int_{I_E} \int_{\Omega} E\mathbb{C}_\nu \boldsymbol{\varepsilon}(\boldsymbol{\rho}_m e_m) \cdot \boldsymbol{\varepsilon}(\boldsymbol{\delta\rho}_m e_m) = \int_{I_E} \int_{\Gamma_N} \mathbf{f} \cdot \boldsymbol{\delta\rho}_m e_m \\ \sum_{i=1}^{m-1} \int_{I_E} \int_{\Omega} E\mathbb{C}_\nu \boldsymbol{\varepsilon}(\boldsymbol{\rho}_i e_i) \cdot \boldsymbol{\varepsilon}(\boldsymbol{\rho}_m \delta e_m) + \int_{I_E} \int_{\Omega} E\mathbb{C}_\nu \boldsymbol{\varepsilon}(\boldsymbol{\rho}_m e_m) \cdot \boldsymbol{\varepsilon}(\boldsymbol{\rho}_m \delta e_m) = \int_{I_E} \int_{\Gamma_N} \mathbf{f} \cdot \boldsymbol{\rho}_m \delta e_m \end{cases} \quad (7)$$

By separating functions, e.g. $\boldsymbol{\varepsilon}(\boldsymbol{\rho}_i e_i) = \boldsymbol{\varepsilon}(\boldsymbol{\rho}_i) e_i$, and grouping functions of the same variable ($\mathbf{x}$ or E) into corresponding integral (over space Ω or interval I_E), the system of equations (8) was obtained. This system of equations was discretized and solved numerically. The spaces Ω and I_E are meshed with n_Ω and n_E elements respectively.

$$\begin{cases} \int_{\Omega} \mathbb{C}_\nu \boldsymbol{\varepsilon}(\boldsymbol{\rho}_m) \cdot \boldsymbol{\varepsilon}(\boldsymbol{\delta\rho}_m) \int_{I_E} E e_m e_m = \int_{I_E} e_m \int_{\Gamma_N} \mathbf{f} \cdot \boldsymbol{\delta\rho}_m - \sum_{i=1}^{m-1} \int_{\Omega} \mathbb{C}_\nu \boldsymbol{\varepsilon}(\boldsymbol{\rho}_i) \cdot \boldsymbol{\varepsilon}(\boldsymbol{\delta\rho}_m) \int_{I_E} E e_i e_m \\ \int_{\Omega} \mathbb{C}_\nu \boldsymbol{\varepsilon}(\boldsymbol{\rho}_m) \cdot \boldsymbol{\varepsilon}(\boldsymbol{\rho}_m) \int_{I_E} E e_m \delta e_m = \int_{I_E} \delta e_m \int_{\Gamma_N} \mathbf{f} \cdot \boldsymbol{\rho}_m - \sum_{i=1}^{m-1} \int_{\Omega} \mathbb{C}_\nu \boldsymbol{\varepsilon}(\boldsymbol{\rho}_i) \cdot \boldsymbol{\varepsilon}(\boldsymbol{\rho}_m) \int_{I_E} E e_i \delta e_m \end{cases} \quad (8)$$

For each element l in the space Ω and each element h in the space I_E, the corresponding elementary functions are written as following:

$$\boldsymbol{\rho}_i^l = \mathbb{N}_{\boldsymbol{\rho}} \mathbf{P}_i^l; \quad \boldsymbol{\delta\rho}_m^l = \mathbb{N}_{\boldsymbol{\rho}} \boldsymbol{\Delta}\mathbf{P}_m^l; \quad e_i^h = \mathbf{N}_e \mathbf{E}_i^h; \quad \boldsymbol{\delta} e_m^h = \mathbf{N}_e \boldsymbol{\Delta}\mathbf{E}_m^h$$

where: $\mathbb{N}_{\boldsymbol{\rho}}$ is the elementary shape function matrix; $\mathbf{P}_i^l$ and $\boldsymbol{\Delta}\mathbf{P}_m^l$ are the elementary (column) vectors of nodal values of displacement field and corresponding test function, respectively. $\mathbf{N}_e$ is an elementary shape function (row) vector for Young's modulus-related problem; $\mathbf{E}_i$ $(i = 1 \ldots m)$ and $\boldsymbol{\Delta}\mathbf{E}_m$ are the elementary vectors of nodal values of functions e_i and corresponding test function, respectively.

Using these discretized forms, all terms of the equation (8) were transformed as follows:

$$\int_{\Omega} \mathbb{C}_\nu \boldsymbol{\varepsilon}(\boldsymbol{\rho}_i) \cdot \boldsymbol{\varepsilon}(\boldsymbol{\delta\rho}_m) = \sum_{l=1}^{n_\Omega} \int_{\Omega^l} \boldsymbol{\varepsilon}^T(\boldsymbol{\delta\rho}_m^l) \mathbb{C}_\nu \boldsymbol{\varepsilon}(\boldsymbol{\rho}_i^l) = \sum_{l=1}^{n_\Omega} \int_{\Omega^l} \boldsymbol{\Delta}\mathbf{P}_m^{lT} \mathbf{d}\mathbb{N}_{\boldsymbol{\rho}}^T \mathbb{C}_\nu \mathbf{d}\mathbb{N}_{\boldsymbol{\rho}} \mathbf{P}_i^l = \boldsymbol{\Delta}\mathbf{P}_m^T \left(\sum_{l=1}^{n_\Omega} \int_{\Omega^l} \mathbf{d}\mathbb{N}_{\boldsymbol{\rho}}^T \mathbb{C}_\nu \mathbf{d}\mathbb{N}_{\boldsymbol{\rho}} \right) \mathbf{P}_i$$

$$\int_{I_E} E e_i e_m = \sum_{h=1}^{n_E} \int_{I_E^h} e_m^{hT} E e_i^h = \sum_{h=1}^{n_E} \int_{I_E^h} \mathbf{E}_m^{hT} \mathbf{N}_e^T E \mathbf{N}_e \mathbf{E}_i^h = \mathbf{E}_m^T \left(\sum_{h=1}^{n_E} \int_{I_E^h} \mathbf{N}_e^T E \mathbf{N}_e \right) \mathbf{E}_i;$$

$$\int_{\Omega} \mathbb{C}_\nu \boldsymbol{\varepsilon}(\boldsymbol{\rho}_i) \cdot \boldsymbol{\varepsilon}(\boldsymbol{\rho}_m) = \mathbf{P}_m^T \left(\sum_{l=1}^{n_l} \int_{\Omega^l} \mathbf{d}\mathbb{N}_{\boldsymbol{\rho}}^T \mathbb{C}_\nu \mathbf{d}\mathbb{N}_{\boldsymbol{\rho}} \right) \mathbf{P}_i; \int_{I_E} E e_i \delta e_m = \boldsymbol{\Delta}\mathbf{E}_m^T \left(\sum_{h=1}^{n_E} \int_{I_E^h} \mathbf{N}_e^T E \mathbf{N}_e \right) \mathbf{E}_i$$

$$\int_{I_E} e_m = \sum_{h=1}^{n_E} \int_{I_E^h} e_m^{hT} = \sum_{h=1}^{n_E} \int_{I_E^h} \mathbf{E}_m^{hT} \mathbf{N}_e^T = \mathbf{E}_m^T \left(\sum_{h=1}^{n_I} \int_{I_E^h} \mathbf{N}_e^T \right); \int_{I_E} \delta e_m = \boldsymbol{\Delta}\mathbf{E}_m^T \left(\sum_{h=1}^{n_I} \int_{I_E^h} \mathbf{N}_e^T \right)$$

$$\int_{\Gamma_N} \mathbf{f}\cdot\boldsymbol{\delta\rho}_m = \int_{\Gamma_N} \left(\boldsymbol{\delta\rho}_m\right)^T \mathbf{f} = \boldsymbol{\Delta P}_m^T \int_{\Gamma_N} \mathbb{N}_{\boldsymbol{\rho}}^T \mathbf{f};\ \int_{\Gamma_N} \mathbf{f}\cdot\boldsymbol{\rho}_m = \mathbf{P}_m^T \int_{\Gamma_N} \mathbb{N}_{\boldsymbol{\rho}}^T \mathbf{f}$$

where $\boldsymbol{\Delta P}_m^T$, $\mathbf{P}_i$, and $\mathbf{P}_m^T$ are the global vectors of nodal values of displacement; $\boldsymbol{\Delta E}_m^T$, $\mathbf{E}_i$, and $\mathbf{E}_m^T$ are the global vectors of nodal values of Young's modulus-related functions.

Denotes

$\mathbb{K}_\nu = \sum_{l=1}^{n_l} \int_{\Omega^l} \mathbf{d}\mathbb{N}_{\boldsymbol{\rho}}^T \mathbb{C}_\nu \mathbf{d}\mathbb{N}_{\boldsymbol{\rho}};\ \ \mathbb{M}_e = \left(\sum_{h=1}^{n_E} \int_{I_E^h} \mathbf{N}_e^T E \mathbf{N}_e \right);\ \ \mathbf{G}_e = \sum_{h=1}^{n_I} \int_{I_E^h} \mathbf{N}_e^T;\ \ \mathbf{F} = \int_{\Gamma_N} \mathbb{N}_{\boldsymbol{\rho}}^T \mathbf{f}$, we have the system of equations in the matrix form as follows:

$$\begin{cases} \left(\boldsymbol{\Delta P}_m^T \mathbb{K}_\nu \mathbf{P}_m\right)\left(\mathbf{E}_m^T \mathbb{M}_e \mathbf{E}_m\right) = \left(\mathbf{E}_m^T \mathbf{G}_e\right)\boldsymbol{\Delta P}_m^T \mathbf{F} - \sum_{i=1}^{m-1} \left(\boldsymbol{\Delta P}_m^T \mathbb{K}_\nu \mathbf{P}_i\right)\left(\mathbf{E}_m^T \mathbb{M}_e \mathbf{E}_i\right) \\ \left(\mathbf{P}_m^T \mathbb{K}_\nu \mathbf{P}_m\right)\left(\boldsymbol{\Delta E}_m^T \mathbb{M}_e \mathbf{E}_m\right) = \left(\boldsymbol{\Delta E}_m^T \mathbf{G}_e\right)\mathbf{P}_m^T \mathbf{F} - \sum_{i=1}^{m-1} \left(\mathbf{P}_m^T \mathbb{K}_\nu \mathbf{P}_i\right)\left(\boldsymbol{\Delta E}_m^T \mathbb{M}_e \mathbf{E}_i\right) \end{cases} \quad (9)$$

Remove the vectors of nodal values of arbitrary test functions ($\boldsymbol{\Delta P}_m^T$ in the first equation and $\boldsymbol{\Delta E}_m^T$ in the second one), the final system of equations (10) is obtained. The unknowns of these equations are $\mathbf{P}_m$ and $\mathbf{E}_m$. These equations are non-linear because the unknowns appear on both sides of each equation. Therefore, this coupled system is solved with a fixed-point algorithm. After initializing $\mathbf{E}_m^{(0)}$, the following computations are iteratively performed: 1 - Compute $\mathbf{P}_m^{(k+1)}$ from $\mathbf{E}_m^{(k)}$ using the first equation; 2 - Compute $\mathbf{E}_m^{(k+1)}$ from computed $\mathbf{P}_m^{(k+1)}$ using the second equation (where *k* denotes iteration index). The iterative process to compute mode *m* may be stopped when it converges (with stagnation of modal functions along iterations) or after a fixed number $k_{\max}$ iterations. In this work, the second way was used.

$$\begin{cases} \left(\mathbb{K}_\nu\right)\left(\mathbf{E}_m^T \mathbb{M}_e \mathbf{E}_m\right)\mathbf{P}_m = \left(\mathbf{E}_m^T \mathbf{G}_e\right)\mathbf{F} - \sum_{i=1}^{m-1} \left(\mathbb{K}_\nu \mathbf{P}_i\right)\left(\mathbf{E}_m^T \mathbb{M}_e \mathbf{E}_i\right) \\ \left(\mathbf{P}_m^T \mathbb{K}_\nu \mathbf{P}_m\right)\left(\mathbb{M}_e\right)\mathbf{E}_m = \mathbf{G}_e\left(\mathbf{P}_m^T \mathbf{F}\right) - \sum_{i=1}^{m-1} \left(\mathbf{P}_m^T \mathbb{K}_\nu \mathbf{P}_i\right)\left(\mathbb{M}_e \mathbf{E}_i\right) \end{cases} \quad (10)$$

The greedy algorithm which was used to find the number of modes consists of adding a new mode to the current solution until reaching the convergence, when the ratio of the norm of the current mode over the norm of the last mode, $\left(\|\mathbf{P}_m\|.\|\mathbf{E}_m\|\right) / \left(\|\mathbf{P}_{m-1}\|.\|\mathbf{E}_{m-1}\|\right)$ is smaller than 10^{-5}.

3. RESULTS AND DISCUSSIONS

In this section, a numerical experiment was performed in order to check the performance of proposed approach.

3.1. Numerical experiment description

Consider a tensile test on a rectangular plate in figure 1. The simulation mesh, which can be seen in the upper part of figure 2 is made of 446 T3 elements. The material is

homogeneous and the objective is to identify Young's modulus E. The DIC displacement $\mathbf{U}_{dic}$ was built numerically by adding to each component i of the FEM displacement $\mathbf{U}^i_{fem}$ obtained from a simulation with the reference set of material coefficients ($E_0 = 200\,\text{GPa},\ \nu_0 = 0.26$) a Gaussian white noise under the form: $\mathbf{U}^i_{dic} = \mathbf{U}^i_{fem} + \eta\gamma_i \mathbf{U}^i_{fem}$ with η the noise level (in this work, 3 levels of noise were considered: $\eta = 10\%,\ 20\%,\ 30\%$) and γ the normally distributed random number. The distribution of $\mathbf{U}_{fem}$, noise (which is $\mathbf{U}_{dic} - \mathbf{U}_{fem}$), and $\mathbf{U}_{dic}$ are presented in the first, second and third columns in figure 4, respectively.

When implementing PGD technique on this problem, the considered range for the values of Young's modulus was from $0.6E_0$ to $1.4E_0$. This range was discretized using a regular mesh of 80 linear 1D elements of $0.01E_0$ length. When computing each mode, a fixed number of iterations $k_{\max} = 4$ was used as in practice the algorithm is converged quickly, therefore it is not necessary to choose a large value for $k_{\max}$.

3.2. Results

The obtained PGD solution, $\mathbf{u}_{pgd}$, consists of 2 modes which are shown in figure 2. This displacement is a function of space coordinates $\mathbf{x}$ and Young's modulus. The sought value of Young's modulus was obtained by minimizing the following cost function which is the Euclidean norm of the difference between vectors of nodal values of $\mathbf{u}_{pgd}$ and $\mathbf{u}_{dic}$:

$$\epsilon(E) = \left[\mathbf{U}_{pgd}(E) - \mathbf{U}_{dic}\right]^T \left[\mathbf{U}_{pgd}(E) - \mathbf{U}_{dic}\right] \tag{11}$$

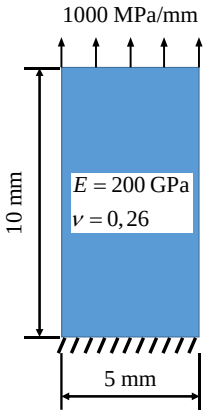

Figure 1. *Test configuration.*

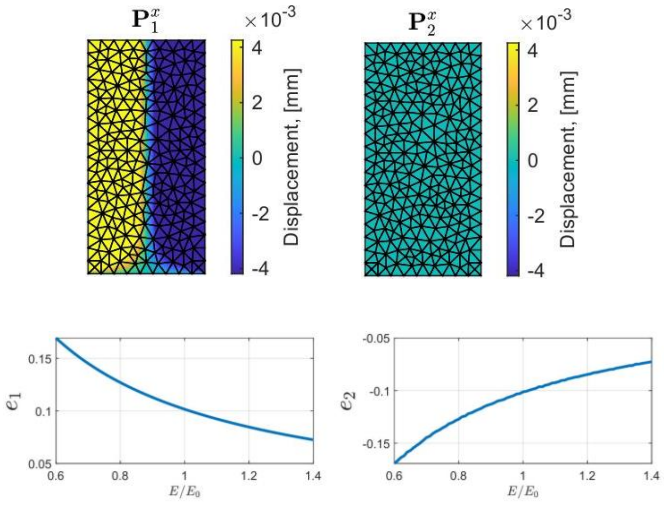

Figure 2. *Modes of PGD solution.*

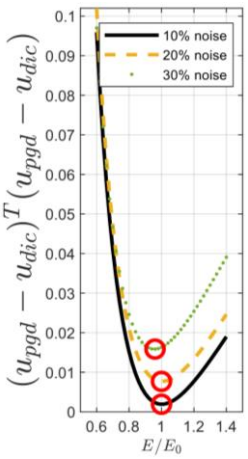

Figure 3. *Cost function.*

The graphics of this function for 3 cases (corresponding to 3 considered levels of noise) are shown in figure 3 where the horizontal axis is normalized. It can be seen that the value of the function changed with the change in noise level. However, noise level

only had a small influence on the value of identified Young's modulus E_{sol} which is the minimizer of the functional: for 10% and 20% of noise, E_{sol} is exactly equal to E_0, for 30% of noise $E_{sol} = 0.96E_0$. For the case of 20% of noise, the displacement field corresponding to E_{sol}, called $\mathbf{u}_{sol}$, is shown in the fourth column of figure 4. In the last column of the same figure is the difference between $\mathbf{u}_{sol}$ and $\mathbf{u}_{dic}$.

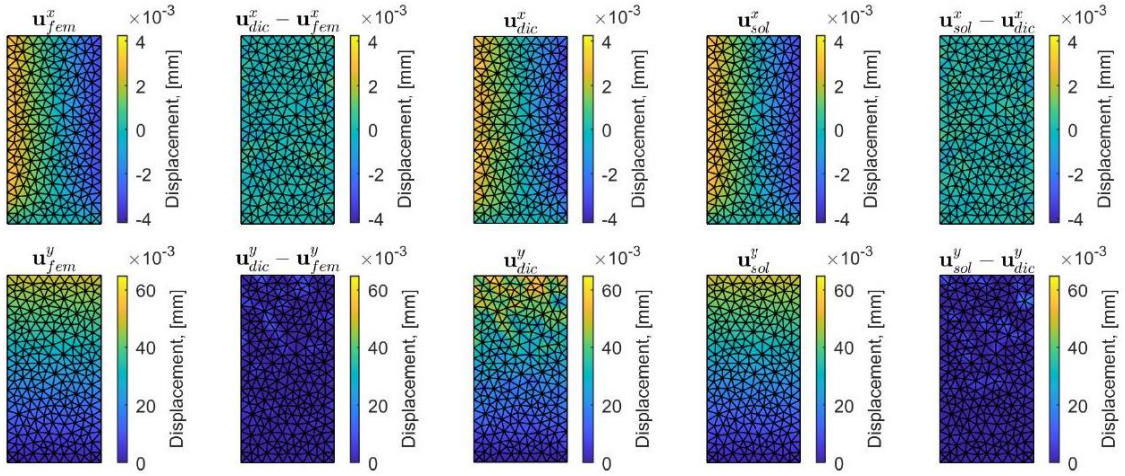

Figure 4. *Different types of displacements.*

3.3. Discussions

As mentioned, there are two ways to stop the iterative process of finding each mode. The way used in this work was fixing the number of iterations which is $k_{\max} = 4$. There are two important points to be drawn. First, the convergence of iterative process was not checked because it was not necessary. Because the system of equations in this work is quite simple; it contains only 2 problems. The fixed-point algorithm in this case has a fast rate of convergence. Therefore, to simplify the code, the procedure of checking convergence was ignored. All of the modes were found after the same number of iterations $k_{\max}$ which was quite small. Practically, there is no need to use a large value for $k_{\max}$. Second, the error in each mode can be compensated by adding the next mode. To stop process of adding mode, the convergence is checked by using its Euclidian norm. That means, the ignorance of convergence checks inside the process of finding each mode enables to avoid doing convergence checks twice in the whole code.

The number of modes of PGD solution is only 2. This confirms the simplicity of the problem and the fast rate of convergence of the fixed-point algorithm. The convergence criterion $\left(\left\|\mathbf{P}^2\right\|.\left\|\mathbf{E}^2\right\|\right) / \left(\left\|\mathbf{P}^1\right\|.\left\|\mathbf{E}^1\right\|\right) < 10^{-5}$ shows that the first mode captures most of the mechanical content of the solution. Although there were only 2 modes in PGD solution, the result of identifying Young's modulus was accurate. It is worth noting that noise has an influence on the identification result but in practice, for the small level, this influence is negligible.

PGD technique enables to use many extra variables. Regarding material parameters, they can be Young's moduli, Poisson's ratios (in total of 2 for isotropic and 4 for

orthotropic material for example). The decomposition of Hooke's matrix depends on these extra parameters. In this work, only one extra parameter, which is Young's modulus, was considered and therefore the decomposition $\mathbb{C} = E\mathbb{C}_\nu$ was used. In this decomposition, $\mathbb{C}_\nu$ is a constant matrix. This made the separation of functions and grouping functions of the same variable easy. If a more complex material is used (e.g. orthotropic or anisotropic), and several parameters need to be identified at the same time, the decomposition of Hooke's matrix will be more complex.

In this work, the effectiveness of using PGD technique was evaluated qualitatively only. The quantitative evaluation can be found in some works, for example [17].

4. CONCLUSIONS

In this study, PGD technique was implemented to solve the material parameter identification problem based on noisy displacement obtained from full-field measurement data using DIC technique. The solution to this problem is material parameters from which the computed displacement matches at best the DIC displacement. In DIC-FEMU approach, which has been widely used, an iterative process of computing displacement has to be performed. By using PGD technique, this task can be avoided as the parameters to be identified are considered as extra-variables of displacement function and this multivariable function, which is approximated in the PGD form, can be evaluated very fast at any values of its variables. Therefore, PGD technique enables to reducing computation costs.

The mathematical formulation of the identification problem using PGD technique was presented. This formulation was then verified by one numerical example of a tensile test. The results showed the high accuracy of the formulation: for the case of 10% and 20% of noise, the value of the identified Young's modulus is exactly equal to the reference one; for the case of 30% of noise, the value of the identified Young's modulus is equal to 96% of the reference one. In addition, the fixed-point algorithm in this case has converged quickly, after only 2 modes even when computing each mode, only a small value for the number of iterations was used.

REFERENCES

[1]. Cailletaud G. and Pilvin P., *"Identification and inverse problems related to material behaviour"*. In H.D. Bui, M. Tanaka, and al., editors, Inverse Problems in Engineering Mechanics (1994).

[2]. Rastogi PK, *"Photomechanics"*, Springer, Berlin (1999).

[3]. Sutton M., *"Computer vision-based, non-contacting deformation measurements in mechanics: a generational transformation"*, Applied Mechanics Reviews, 65(5):050000, (2013).

[4]. Hild F. and Roux S., *"Digital image correlation"*, In *"Optical Methods for Solid Mechanics. A Full-Field Approach"*, Wiley, pages 183–228, (2012).

[5]. Avril et al., *"Overview of identification methods of mechanical parameters based on full-field measurements"*, Experimental Mechanics, 48:381–402, (2008).

[6]. Hai Nam Nguyen et al, *"mCRE-based parameter identification from full-field measurements: Consistent framework, integrated version, and extension to nonlinear"*, Computer Methods in Applied Mechanics and Engineering, Volume 400, 115461, (2022).

[7]. Pagnacco E. et al., *"Inverse strategy from displacement field measurement and distributed forces using FEA"*. In *"2005 SEM annual conference and exposition on experimental and applied mechanics"*, Portland, (2005).

[8]. Chatterjee A., *"An introduction to the proper orthogonal decomposition"*, Current Science, 78(7):808–817, (2000).
[9]. Maday Y. and Ronquist E., *"A reduced-basis element method"*, Comptes-Rendus de l"Académie des Sciences, I, Paris, 335:195–200, (2002).
[10]. Chinesta F. et al., *"The proper generalized decomposition for advanced numerical simulation"*, Springer, (2014).
[11]. Chinesta F. et al., *"Recent Advances and New Challenges in the Use of the Proper Generalized Decomposition for Solving Multidimensional Models"*, Arch Comput Methods Eng 17: 327–350, (2010).
[12]. Hasini Garikapati, *"A Proper Generalized Decomposition (PGD) approach to crack propagation in brittle materials: with application to random field material properties"*, Computational Mechanics 65:451–473, (2020).
[13]. P. Z. Qin, *"Finite Element Modeling and PGD Based Model Reduction for Piezoelectric & Magnetostrictive Materials"*, Doctoral Thesis, Université Pierre et Marie Curie, (2016).
[14]. K. El-Ghamrawy, S. Zlotnik, *"Proper generalized decomposition solutions for composite laminates parametrized with fibre orientations"*, Comput Mech 71, 89–105, (2023).
[15]. M. El Fallaki Idrissi, *"Multiparametric modeling of composite materials based on non-intrusive PGD informed by multiscale analyses: Application for real-time stiffness prediction of woven composites"*, Composite Structures, Volume 302, 116228, (2022).
[16]. Allier P. E. et al, *"Proper generalized decomposition computational methods on a benchmark problem: introducing a new strategy based on constitutive relation error minimization"*, Adv Model Simul Eng Sci. 2(17), (2015).
[17]. P. E. Allier et al., *"Towards simplified and optimized a posteriori error estimation using PGD reduced models"*, Int J Numer Meth Engng. 113:967–998, (2018).

TÓM TẮT

Áp dụng kỹ thuật PGD trong việc giải bài toán xác định mô đun đàn hồi của vật liệu đàn hồi tuyến tính đẳng hướng từ dữ liệu đo toàn trường bằng phương pháp FEMU

Bài báo trình bày việc áp dụng kỹ thuật PGD trong việc giải bài toán xác định mô đun đàn hồi của vật liệu đàn hồi tuyến tính đẳng hướng từ dữ liệu đo toàn trường bằng phương pháp FEMU. Đối với dạng bài toán này, việc sử dụng kỹ thuật PGD cho phép giảm chi phí tính toán vì nó giúp tránh phải thực hiện quá trình lặp để tính toán đáp ứng của kết cấu cơ học bằng phương pháp phần tử hữu hạn (FEM). Bản chất của kỹ thuật PGD nằm ở những điểm quan trọng sau: (i) – Các tham số được quan tâm sẽ được coi như là các biến bổ sung đối với với hàm đáp ứng; (ii) – Hàm đáp ứng nhiều chiều cần tìm được xấp xỉ bằng tổng hữu hạn các mode, mỗi mode là tích của các hàm đơn biến tách biệt; (iii) – Nghiệm xấp xỉ này được tính bằng một bộ giải lặp, sử dụng nguyên lý biến phân và thuật toán greedy. Một ví dụ số trên một thử nghiệm kéo đã được thực hiện để kiểm chứng việc áp dụng này. Các kết quả thu được đã khẳng định sử đúng đắn của kỹ thuật PGD. Một số nhận xét về việc sử dụng kỹ thuật này đã được đưa ra.

Từ khoá: Bài toán xác định tham số vật liệu; Phương pháp FEMU; Kỹ thuật PGD.